Microchimica Acta (2020) 187:72
https://doi.org/10.1007/s00604-019-4026-0

ORIGINAL PAPER

A metal-organic zeolitic framework with immobilized urease for use in a tapered optical fiber urea biosensor

Guixian Zhu[1] · Lin Cheng[1] · Ruogu Qi[2] · Mizhen Zhang[1] · Jiahao Zhao[3] · Lianqing Zhu[1,4] · Mingli Dong[1]

Received: 9 July 2019 / Accepted: 9 November 2019
© Springer-Verlag GmbH Austria, part of Springer Nature 2019

Abstract

A tapered single-mode coreless single-mode (SCS) structure with high sensitivity for sensing refractive index is described. In order to achieve high specificity of optical biosensors, here enzyme capsulation film was achieved by embedding urease in zeolitic imidazolate framework (ZIF-8/urease) through in situ growth approach on the coreless fibers. Determination of urea is achieved through online monitoring of its binding to the urease in zeolitic imidazolate framework. Refractive index change result in wavelength shifts of the optical fiber biosensor. The resonance wavelength exhibits a good linear relationship with urea concentration in the range of 1 to 10 mM with detection limit of 0.1 mM and sensitivity of 0.8 mM/RIU (refractive index unit) if operated with broadband light ranging from 1525 nm to 1590 nm. Final assessment of optical biosensor in real sample was performed where excellent performance in terms of sensitivity and selectivity was observed.

Keywords Single-mode coreless single-mode structure · Refractive index · Enzyme capsulation · Biorecognition layer · Label free detection

Introduction

Optical fiber biosensors are significant in measuring refractive index [1–3], temperature [4, 5], pressure [6] and curvature [7] due to their low cost and convenient processing [8, 9]. Standard optical fibers, composed by core and cladding, show limitations in sensing due to confinement of optical field by thick cladding. Various structures such as grating-assisted [2, 10, 11], surface plasmon resonance [12–16] and tapering fibers [17–19] have been developed to strength the evanescent field or multimode interference. The principle of single-mode multimode single-mode (SMS) is multimode interference [20]. The enhanced evanescent field is achieved after tapering, which leads to higher sensitivity of the fiber. However, the cladding of multimode fibers is needed to removed, which dramatically increase the fabrication difficulty. In order to improve the reliability of SMS structure, the coreless fiber (CF) is applied and spiced between two simple-mode fibers (SMF), forming single-mode coreless single-mode (SCS) structure [21].

Besides sensitive optical fiber structures, another key element of optical sensors is selective sensing layer that captures analytes. Antibodies [22], DNA [23] and enzyme [24, 25] can be modified on optical fibers as molecular recognition elements. Metal organic frameworks (MOFs), as crystalline materials with large surface areas, tunable pore size and high affinity, have been applied for encapsulating bioactive molecules to form sensitive biorecognition films [26]. Compared with other matrices, MOFs have been reported to protect biomolecules from high temperature and organic solvents [27, 28]. The open porous architectures of MOFs also enable the selective interaction of biomolecules (for example, enzymes)

Electronic supplementary material The online version of this article (https://doi.org/10.1007/s00604-019-4026-0) contains supplementary material, which is available to authorized users.

✉ Guixian Zhu
zhuguixian0514@163.com

✉ Mingli Dong
ztsxnl@126.com

[1] School of Instrument Science and Opto-electronics Engineering, Beijing information Science and Technology University, Beijing 100192, China

[2] Department of Nanomedicine, Houston Methodist Research Institute, Houston, TX 77030, USA

[3] Beijing Innovation Center for Future Chips, Tsinghua University, Beijing 100084, China

[4] School of Instrument and Opto-electronics Engineering, Hefei University of Technology, Anhui 230009, China

with analytes through their selective transport in the porous coating [29].

Zeolitic imidazolate framework (ZIF-8), a representative Zn based MOF, is chosen as a matrix for urease immobilization. Here a new optical biosensor based on ZIF-8/urease sensing film is demonstrated. SCS structure is applied as the optical device to detect refractive index change of analytes, and ZIF-8/urease is used for urea biorecognition. All the parts enable sensitive identification of urea. The strategy is also applicable for other enzymes and various kinds of enzyme based optical sensor would be further developed.

Experimental section

Fabrication of the single-mode coreless single-mode (SCS) optical fiber

IThe coreless fiber (CF; typeFud-3582, Nufern, length: 2 cm) was spliced and placed in middle of two SMFs (SMF-28, Corning), forming SCS structure. Then the CF in SCS was tapered by CO_2 laser splicing machine (LZM-100, Fujikura) to form tapered SCS optical fiber. beam propagating method (BPM) was applied to simulate optical field distribution and transmission spectra of tapered SCS structure. For the spectral measurement setup, two SMFs were placed in middle of the broadband light source (BBS) and optical spectrum analyzer (OSA, AQ6370, Yokogawa). A microfluidic device was used as the sample cell.

Synthesis ZIF-8 and ZIF-8/urease

ZIF-8 was prepared by rapid aqueous synthesis method. Briefly, an equal volume of zinc nitrate (40 mM) and 2-methylimidazole (160 mM) was prepared in deionized (DI) water for 30 min. The formed product was collected and washed twice with water and dried.

In order to obtain urease embedded composite, A water solution (20 μL) of urease (50 $mg{\cdot}mL^{-1}$) and zinc nitrate solution (40 mM, 200 μL) were mixed with same volume of 2-methylimidazole (160 mM) at room temperature. After 30 min, the product was collected and washed with DI water for three times and dried. The effect of initial reagents of Zn^{2+} and 2-MIM was also investigated by changing parameters in reaction.

The loading efficiency of composites for urease was calculated. The protein concentration was determined by Bradford assay. Commercially Bradford assay kit was purchased from Solarbio, inc, and the protein concentration was measured and calculated according to the standard protocol.

All morphologies of product were observed by scanning electron microscope (SEM). Samples were suspended in ethanol and 2 μL was dropped on a silicon wafer. A thin layer (2 nm) of gold film was sputtered on samples to enhance electrical conductivity.

Urease activity assay

30 $mg{\cdot}mL^{-1}$ urea in 2 mL phosophate buffered saline (PBS) (pH 7.4) and 30 μL 1 $mg{\cdot}mL^{-1}$ phenol red was added to a cuvette. Then the cuvette was placed in the UV spectrometer. After 2 min, the absorbance set to zero to establish a baseline. 60 μL ZIF-8/urease suspension was added. The increase in the absorbance at 560 nm along with time was recorded to measure the urease activity.

Surface modification of ZIF-8/urease on tapered SCS optical fiber

Before ZIF-8/urease coating process, CF in SCS structure was treat with 1% polystyrene sulfonate solution at room temperature for 24 h. The modified SCS was immersed in aqueous solution of 2-methylimidazole (160 mM, 200 μL), then 20 μL of urease (50 $mg{\cdot}mL^{-1}$) and zinc nitrate solution (40 mM, 200 μL) were added and reacted for 30 min. The modified SCS fiber was washed with DI water for three times to remove excess isolated composites in solutions.

Urea analysis by tapped SCS optical fiber

Various concentrations of urea in PBS were prepared and their refractive indices were determined by using Abbe refractometer. 50 μL urea solutions with different concentrations (0, 2, 4, 6, 8, 10 mM) were dropped on a microfluidic sample cell and related transmission spectra at wavelength range (1540–1580 nm) were recorded. For an unknown sample (for example: urine). Urine samples were centrifuged at first to remove impurities. Then samples were diluted 50-fold in distilled water prior to assay. Then 50 μL samples were dropped on the sample cell. The transmission spectra (wavelength range: 1540–1580 nm) before and after sample loading were recorded.

Results and discussion

ZIF-8/urease synthesis and characterization

Immobilization strategies can improve the thermal and chemical stability of biomolecules against harsh conditions [26]. MOFs have been extensively investigated for enzyme encapsulation because of their large surface area, tunable porosity and high thermal stability. The porous nature of MOF also facilitate reaction between enzymes with analytes [30]. Most MOFs are synthetized in organic solvents or at high thermal conditions, which denature enzymes. As a representative MOF, ZIF-8 is most frequently used for enzyme encapsulation due to their high stability, biocompatibility, easy to synthesis under mind conditions (at room temperature) and easy to

control the morphology during synthesis [31]. Therefore, ZIF-8 is chosen for urease encapsulation.

Urease embedded ZIF-8 composites were obtained via in-situ synthesis method. Enzyme molecules are either physically absorbed and covalently bound to support matrix by previous report [32]. By applying MOFs, enzyme can be loaded via in-situ synthesis method, in which MOF are formed in the presence of enzyme. Urease was used as a model protein. After being encapsulated into ZIF-8, urease reserved its catalytic activity. Bradford assay was applied to calculate amounts of urease [28]. Results in Fig. 1a show that ZIF-8 exhibit high loading capability for urease, more than 800 μg/mg. To ascertain that urease is encapsulated in crystalline structure, samples were washed to remove surficial enzymes and precipitate was measured by Fourier transform infrared spectroscopy (FTIR). As shown in Fig. 1b, the stretches of urease at 1640–1660 cm^{-1} is corresponding to amide I (C=O stretching mode), while no stretches of protein is shown for free ZIF-8. Additional evidence of urease encapsulation was confirmed by Bradford assay, in which no urease was found in surfactant. The X-ray diffraction (XRD) patterns reveal that there is no obvious difference between the ZIF-8 and ZIF-8/urease samples (shown in supporting information Fig. S1). The nitrogen sorption isotherms were applied to investigate the porous features of samples. As shown in Fig. S2, ZIF-8/urease shows a smaller total pore volume compared to pure ZIF-8 due to occupation of urease in porous structure of ZIF-8. Thermogravimetric analysis (TGA) curves of samples are shown in Fig. 1c, in which ZIF-8/urease a deeper drop above 320 C^o due to decomposition of urease in ZIF-8/urease. The loading amount of urease was calculated to be around 10 wt%, indicating successful loading of urease in the composites.

In order to know the distribution of urease loaded in ZIF-8 structure, Urease molecules were linked with fluorescent label (FITC) and embedded in ZIF-8 during reaction. Urease-FITC on ZIF-8 particles were also prepared though physically mixing for comparison. The synthetized Urease-FITC on ZIF-8 and ZIF-8/urease-FITC were observed by confocal microscope and results are shown in Fig. 1d and Fig. 1e. The confocal microscope images show a clear difference between two samples. For urease-FITC on ZIF-8, green fluorescence is distributed on external surfaces of ZIF-8 crystals. The urease-FITC molecules are distributed more homogeneously with in ZIF-8/urease-FITC samples, indicating that urease molecules are embedded in ZIF-8 during reaction.

Urease is known to be sensitive to inhibition by heavy metal ions. Enzyme activity of urease in ZIF-8/urease has been carried out and results are shown in Fig. S3. ZIF-8/urease, free urease and Zn^{2+}+urease show similar enzymatic rate of reaction in the assay, indicating negligible impact of ZIF-8 and Zn^{2+} on activity of urease.

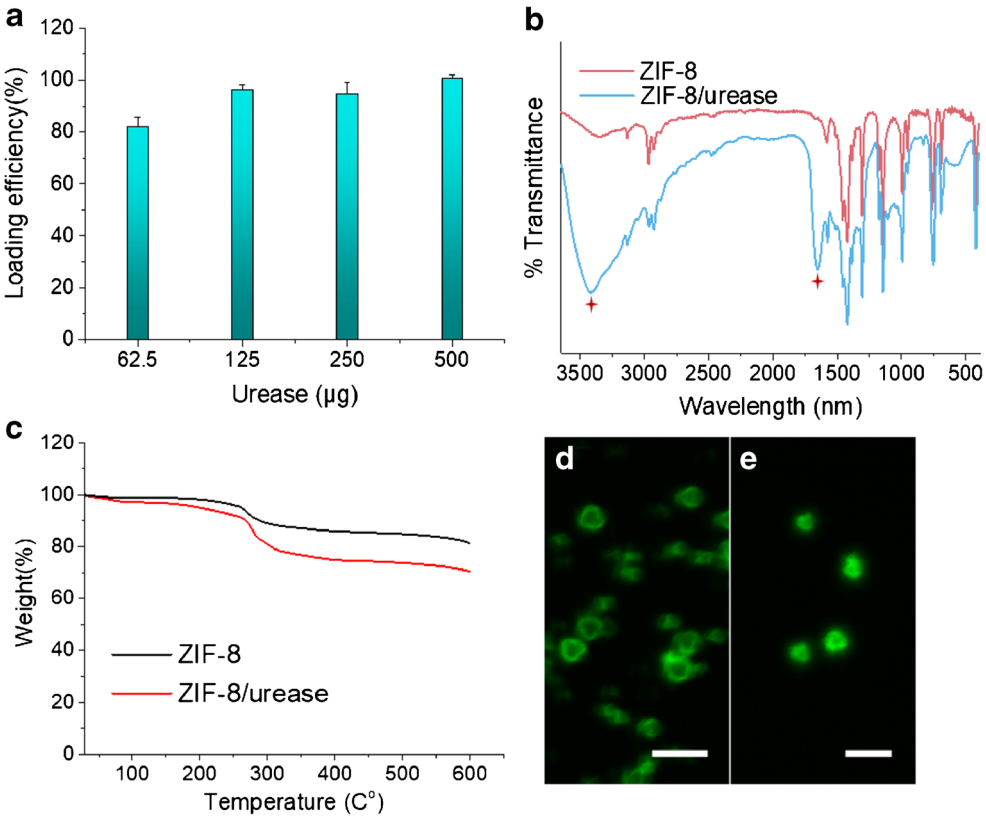

Fig. 1 **a** Loading efficiency of urease in ZIF-8 with different concentrations of urease; **b** FTIR spectra of free ZIF-8 and ZIF-8/urease; **c** thermogravimetric analysis (TGA) curves of free ZIF-8 and ZIF-8/urease and confocal microscope images of (**d**) urease-FITC on ZIF-8 and (**e**) ZIF-8/urease-FITC, scale bar: 2 μm

Micronano SCS optical fiber simulation and fabrication

Here a tapered SCS (single-mode coreless single-mode) fiber is designed for sensing refractive index. Coreless fiber is placed in middle of two single-mode fibers, then the coreless fiber in SCS is tapered by CO_2 laser (LZM-100, Fujikura) to obtain tapered SCS structure (shown in Fig. 2a). The diameters of tapered coreless fibers are adjustable by changing fabrication parameters. The beam propagating method (BPM), based on scalar Helmholtz equation, is used to simulate the distribution of optical field (shown in Fig. 2b), in which SCS fiber with a waist diameter of 10 μm. There is change of optical field and generation of self-image effects at the splicing point between SMF and CF, respectively.

Multimode interference is the principle for SCS structure. Due to core mismatch, the interference happens when the lights transfer from SMF to CF. The transmission spectrum can be expressed as:

$$I(\lambda) = \sum_{m=1}^{N} {c_m}^2 I_0(\lambda) + \sum_{i \neq j=1}^{N} c_i \cdot c_j I_0(\lambda) \cdot \cos\left(\beta_i - \beta_j\right) \cdot L \qquad (1)$$

Where β is longitudinal propagation constant, c is the excitation coefficient of eigenmode, and L is the length of CF. The change of RI has an influence on β and c in Eq. (1), resulting in changes of output spectra. Therefore, the RI can be calculated via monitoring spectral changes.

Previous study shows there is an exponential fitting between RI and related wavelength shifts of CF spectra. Various diameters of CF (length: 2 cm) in SCS were fabricated to analyze their influence on RI sensitivity. The SCS fiber, fixed in microfluidic sample cell, was placed between a laser source and an optical spectrum analyzer (OSA, Yokagawa).

The sensitivity of SCS sensor increases obviously as waist diameter decreases. The samples with different RI were dropped on sample cell and resulted spectra of SCS sensor are shown in Fig. 2c. Sensitivity of SCS structure (diameter 20 nm) with RI range of 1.333–1.339 is about 653 nm/RIU while is up to 2083 nm/RIU for SCS with 10 μm diameter. The RI sensitivity of SCS (diameter: 10 μm) increases up to almost 26 times compared with non-tapered SCS (diameter: 125 μm). The transmission spectra of SCS along with urea concentrations was also investigated. Abbe refractometer is applied to measure refractive indices of urea solutions (shown in Fig. S4). As displayed in Fig. 2d, Resonance wavelength demonstrate red shifts with increasing urea concentrations, which is in accordance with results in Fig. 2b. However, there is little change of RI for urea molecules at low concentrations (only 0.0001 from DI water to 10 mM urea). SCS fibers coated with free ZIF-8 show about 0.13 nm wavelength shift with 10 mM urea, which is insufficient to detect urea at biological range. Therefore, ZIF-8/urease composites are applied on fibers for signal amplification and specific recognition for sensing urea.

Urease loading efficiency

ZIF-8 shows great capability for loading urease. Ratio of 2-MIM/Zn^{2+} and their initial concentration in system exhibit a great impact on properties of final ZIF-8. Precious studies

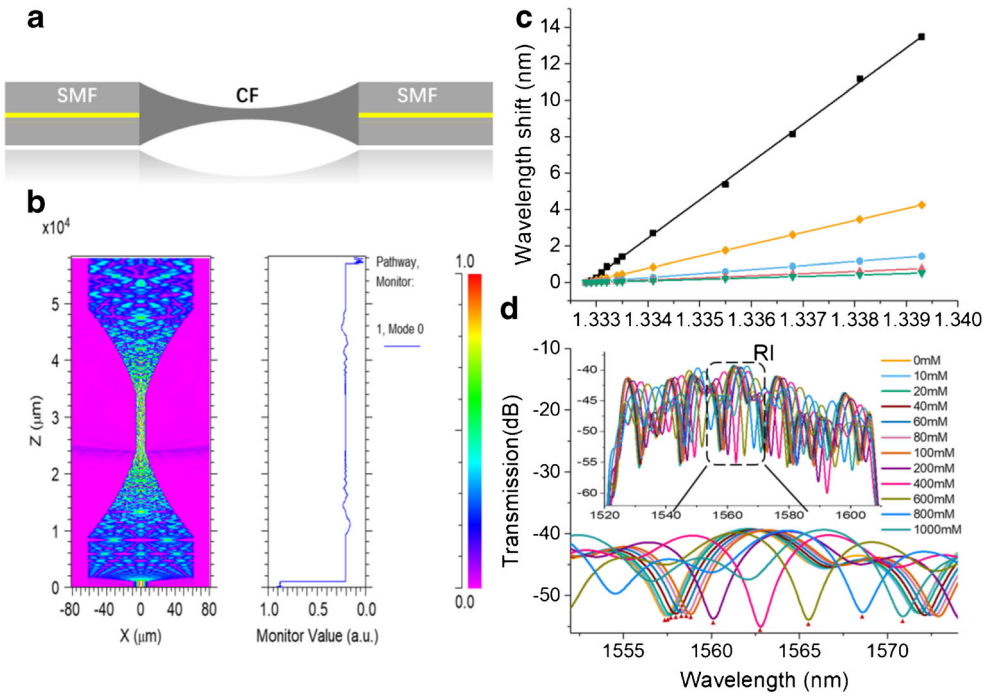

Fig. 2 **a** schematic diagram of SCS fiber; **b** optical field distribution of SCS structure; **c** different diameters (coreless part) to different diameters (coreless part: black, 10 μm; yellow, 20 μm; blue, 40 μm; red, 80 μm and green, 125 μm)(**d**) transmission spectra of SCS (diameter: 10 μm) with various concentrations of urea

report that there is a dependence relationship between morphologies of ZIF-8 composites and concentrations of 2-MIM/Zn^{2+}.The initial concentrations of urease and Zn^{2+} is fixed (40 mM) while changing 2-MIM concentrations. The loading efficiency is determined by Bradford assay, and standard curve is displayed in Fig. S5 and morphologies of products were further characterized by scattering electron microscope (SEM). As shown in Fig. 3a-b and Fig. S6, there is an obvious change of structures with different initial 2-MIM concentrations, which may due to urease affinity towards 2-MIM via hydrogen bonding and hydrophobic interactions. Previous study reported that biomacromolecules have an impact on final crystalline structure of metal organic frameworks [26]. Free ZIF-8 exhibit different morphologies synthetized under same condition (displayed in Fig. S7a-d). Leaf-like structures and rough spheres are obtained for free ZIF-8 instead of needle-like structures for ZIF-8/urease. Results in Fig. 3c shows that the composite achieved almost 100% loading efficiency of urease when ratio of 2-MIM/Zn^{2+} is below 10:1. However, a decrease tendency happens with a further increase in ratio of 2-MIM/Zn^{2+}. Less than 50% of urease is encapsulated in ZIF-8 when this ratio is 40:1.

The effect of initial concentrations of $Zn^{2+}$and 2-MIM were also investigated. Briefly, the ratio of 2-MIM/ Zn^{2+} is 4:1, and the Zn^{2+} concentrations range from 40 to 200 mM while concentrations of 2-MIM were changed from 160 mM to 800 mM correspondingly. The morphologies of composites (320:80) were observed by SEM. Popcorn and leaf-Like composited are obtained as shown by SEM images (Fig. 3d-e and Fig. S6d-f). Angles on structure of products decrease with increasing initial $Zn^{2+}$and 2-MIM concentrations. Popcorn-shape composited are obtained when initial concentrations of Zn^{2+} below 120 mM and 2-MIM below 480 mM, while rough spheres are formed for control sample (Fig. S7e, f). Leaf-like structures are formed with higher initial concentrations (Fig. S7 g, h).

For urease encapsulation, increasing initial concentrations lead to decreasing loading efficiency (shown in Fig. 3f). Full enzyme encapsulation is achieved when Zn^{2+} less than 80 mM and 2-MIM less than 320 mM. A dropping tendency of loading efficiency occurs with raising initial concentrations. Less than 40% loading efficiency is obtained for 200 mM of Zn^{2+} and 800 mM of 2-MIM. The ZIF-8-enzyme interaction were affected by interaction between Zn^{2+} and carbonyl groups of enzymes, which induces nucleation and growth of ZIF-8 with low initial Zn^{2+} and 2-MIM concentrations. Higher Zn^{2+} and 2-MIM lead to lower enzyme encapsulation due to direct crystal formation with less promotion of ZIF-8-enzyme interaction.

ZIF-8/urease optical fiber modification

Integration of ZIF-8/urease as coatings on SCS structure leads to functional sensing films. ZIF-8/urease were deposited on SCS by in-site crystallization approach. Briefly, negatively charged SCS fiber, modified by polystyrene sulfonate (PSS) solutions, were immersed in reacting solution (Zn^{2+}, 2-MIM and urease) for 30 min. Transmission spectra for ZIF-8/urease growth on fibers were monitored and displayed in Fig. 4a, which shows that red shift of resonance wavelength happens

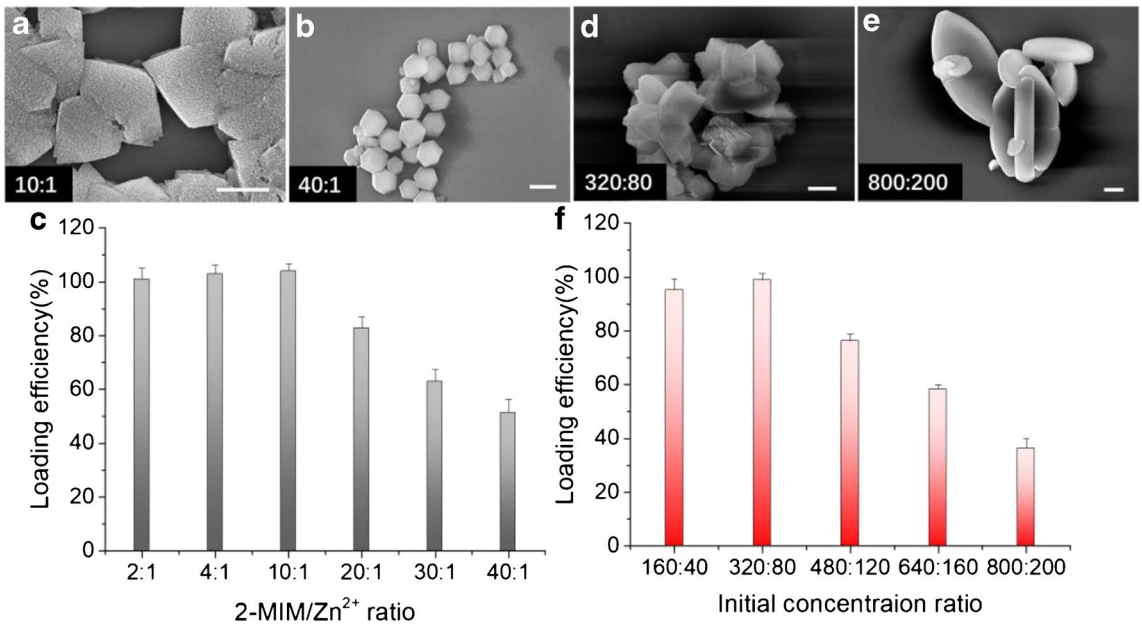

Fig. 3 **a**, **b** SEM images of ZIF-8/urease and (**c**) related loading efficiency of urease with different 2-MIM/Zn^{2+} ratio (a 10:1; b, 40:1); **d**, **e** SEM images of ZIF-8/urease and (**f**) related loading efficiency of urease with different initial concentration of 2-MIM and Zn^{2+} (c 320:80; d, 800:200). Scale bar: 1 μm.

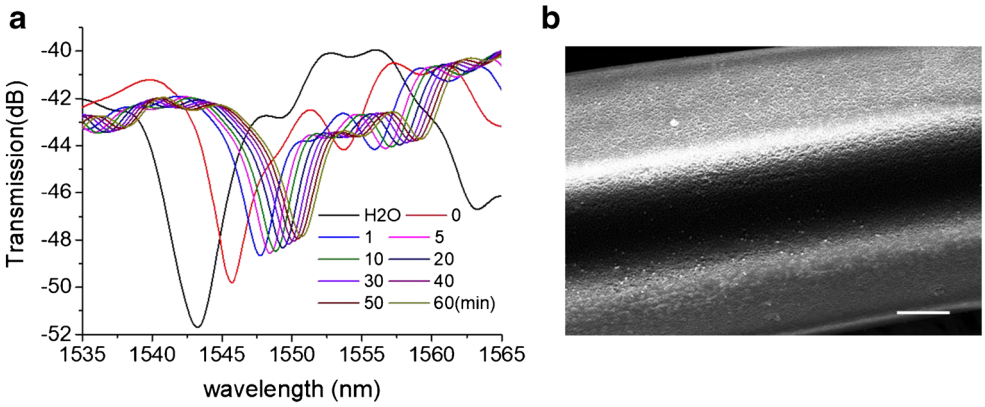

Fig. 4 **a** transmission spectra of single-mode coreless single-mode (SCS) with ZIF-8/urease along with time; **b** SEM image of ZIF-8/urease film on coreless fiber in SCS structure after 60 min, scale bar:20 μm

as reaction time increases, indicating formation of ZIF-8/urease film. A decrease of peak intensities happens due to RI induced variation of coupling coefficient. The transmission spectra of ZIF-8 growth on SCS has been shown in Fig. S8 for comparison. There is no significant change in transmission spectra along with time for ZIF-8 growth on SCS (2-MIM/ Zn^{2+}: 80:20). The ZIF-8/urease composites can be formed rapidly after mixing because of promoting nucleation of urease. For free ZIF-8, the process of crystal formation is greatly delayed. Therefore, there is no obvious change of the transmission spectra of ZIF-8 growth on SCS. SEM image in Fig. 4b shows successful deposition of uniform and dense ZIF-8/urease film on fiber (2-MIM/ Zn^{2+}: 80:20). Modification morphologies of modified Fibers with different initial 2-MIM/ Zn^{2+} were observed by SEM and shown in Fig. S9.

Urea analysis

The sensing mechanism of biosensor for urea is shown in Fig. 5a. ammonia and carbon dioxide will be produced when the urea is oxidized with urease in ZIF-8. The RI surrounding SCS fiber changes with urea addition, leading to resonant wavelength shifts.

The performance of SCS optical biosensor is calculated. The sensor probe was exposed to various concentrations of urea (range from 0 to 10 mM), and corresponding resonant spectra were recorded (Fig. 5b) The SCS fibers coated with ZIF-8/urease shows stronger wavelength resonance in comparison with fibers mixed with free urease and ZIF-8. ZIF-8/urease is highly specific to detection of urea. There is only about 1.2 nm and 0.15 nm wavelength shift for optical fibers with free urease and free ZIF-8 respectively. The RI of 10 mM urea molecules is 1.3329 at room temperature, while the RI of DI water is 1.3328 under same conditions. There is little change of RI for urea molecules at low concentrations. Therefore, SCS fibers coated with free ZIF-8 show smaller wavelength shift at low concentrations of urea. However, the value for ZIF-8/urease coated SCS fibers is increased to 8.0 nm. It is noted that modified SCS shows a linear relationship with urea concentrations range from 1 mM to 10 mM, which covers biological range for human. To investigate mechanism of resonance wavelength shift, it is significant to know the interaction of urea molecules with urease at the modified sensing layer. The hydrolysis of urea requires direct contract between urease sensing layer and urea on optical fibers. The concentrations of urea have an impact on hydrolytic rate. Accumulation and change of urea and products

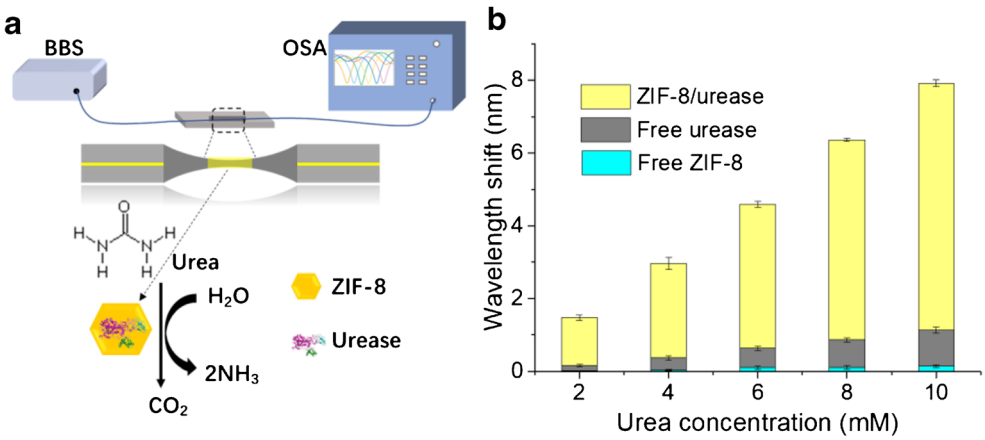

Fig. 5 **a** experimental setup and mechanism for urea detection, **b** corresponding resonant wavelength shift with different urea concentrations

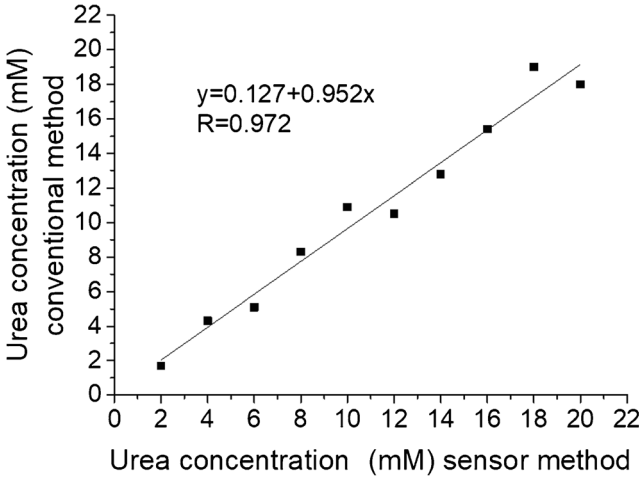

Fig. 6 Correlation of results of urea determination obtained using present optical biosensor and conventional method

result in obvious increase interfacial thickness and RI of biorecognition layer, which further results in red shift of wavelength resonance. Negligible change in resonance wavelength was observed without biosensing layer on SCS fibers, confirming importance of biorecognition layer.

It is significant to apply the designed device in real samples. The response of this designed biosensor for urea in urine was carried out and results are shown in Fig. S10. Since urine contains far more urea than blood samples, the urine samples need to be diluted before testing. There is a good relationship between resonance wavelength and urea concentrations, indicating the designed optical fiber has potential application for urea detection in urine. Although there are some impurities, the high dilution ratio of urine sample could reduce their effect. The composition of urine is simpler compared with plasma. The proteins, peptides and other nutrients may have some serious effect on test results, which need our further investigation. The efficacy of optical sensor for urine samples was also investigated and compared with conventional method using urea assay kit. As shown in Fig. 6, urea concentrations obtained by applying these two methods are statistically same, which is calculated by student's method. The correlation equation was: $y = 0.127 + 0.952x$ with correlation coefficient 0.972.

Table 1 displays sensing performance comparing with previous reports [36]. The sensitivity of our sensor is about 0.8 nm/mM, which is about 4 times higher than SPR method. Compared with other studies by applying silica nanoparticles or Ag/Au as coating matrices, the method applied realizes narrower sensing range (1–10 mM), which covers biological level for human blood urea between 2.8–7.2 mM. In-situ growth of ZIF-8/urease ensure the film uniformity, which is more difficult for spreading of polymer on optical fibers. The large surface area and porous structure of ZIF-8 enhance enzyme loading and substrate diffusion in the matrix, as a result, higher enzyme activity can be achieved. Previous studies have demonstrated that metal organic frameworks show superior protection for enzymes under harsh conditions [26, 31, 37]. ZIF-8 protection extends bioactive temperature range of urease compared with free urease. Therefore, the biorecognition layers can not only realize selective urease identification but also realize urease protection.

The diameters of CF show great influence for sensitivity of SCS structure. Lower diameter achieves higher optical sensitivity. However, the mechanical property of SCS structure becomes breakable due to ultra-small diameters, which is the big challenge for further applications. Therefore, how to improve the stability of SCS needs further investigation. A lab-on-a-chip system, integrating urea optical fiber biosensors with microfluidic channels can be a feasible method, which need our further investigation.

Conclusion

ZIF-8/urease was applied as a biorecognition layer on tapered SCS optical fibers to achieve label-free urea detection in the low concentration level. Tapered SCS structure was demonstrated to be sensitive to surrounding refractive index whose sensitivity is up to 2083 nm/RIU, the ZIF-8 crystals with high surface area were applied to provide a favorable platform for urease immobilization. The designed optical biosensor shows a linear response with sensitivity of ~0.8 nm/mM at low urea concentration range of 1–10 mM. Compared with other sensors, the present sensor shows advantages in fast response, label free detection and compactness. To overcome the signal instability, this device can be integrated in a microfluidic chip for further biosensing applications.

Table 1 Nanomaterial-based optical methods for the determination of urea

Materials used	Immobilization method	Optical detection method	Sensing range	Urea Sensitivity	References
Silica nanoparticles	Covalent bonding	Reflectance spectrophotometric	5-500 mM	About 0.39 a.u/mM	[33]
PANI/cellulose polyacetate	Encapsulation	UV/Vis spectrophotometric	1-10 mM	–	[34]
Au/Ag	Covalent bonding	SPR fiber biosensor	1-160 mM	About 0.2 nm/mM	[35]
ZIF-8 (this method)	Encapsulation	Optical fiber biosensor	1-10 mM	About 0.8 nm/mM	This work

Acknowledgments The authors acknowledge financial support from the following sources: National Natural Science Foundation of China Grant (61805016; 61735002); National Key R&D Program of China (2018YFF01012000); Research Fund from Beijing Innovation Center for Future Chips, General Project of Science and Technology Plan of Beijing Education Commission and Key Cultivation Projects of Beijing Information Science and Technology University.

References

1. Li L, Liang Y, Liu Q, Peng W (2016) Dual-Channel Fiber-optic biosensor for self-compensated refractive index measurement. IEEE Photon Technol Lett 28(19):2110–2113
2. Baliyan A, Sital S, Tiwari U, Gupta R, Sharma EK (2016) Long period fiber grating based sensor for the detection of triacylglycerides. Biosens Bioelectron 79:693–700
3. André RM, Warren-Smith SC, Becker M, Dellith J, Rothhardt M, Zibaii MI, Latifi H, Marques MB, Bartelt H, Frazão O (2016) Simultaneous measurement of temperature and refractive index using focused ion beam milled Fabry-Perot cavities in optical fiber micro-tips. Opt Express 24(13):14053–14065
4. Zhang S, Zhao Z, Chen N, Pang F, Chen Z, Liu Y, Wang T (2015) Temperature characteristics of silicon core optical fiber Fabry-Perot interferometer. Opt Lett 40(7):1362–1365
5. Hao S, Hu M, Rong Q, Du Y, Yang H, Qiao X (2014) High sensitivity optical fiber temperature sensor based on the temperature cross-sensitivity feature of RI-sensitive device. Opt Commun 323(14):28–31
6. Xu J, Pickrell G, Wang X, Wei P, Cooper K, Wang A (2005) A novel temperature-insensitive optical fiber pressure sensor for harsh environments. IEEE Photon Technol Lett 17(4):870–872
7. Monzon-Hernandez D, Martinez-Rios A, Torres-Gomez I, Salceda-Delgado G (2011) Compact optical fiber curvature sensor based on concatenating two tapers. Opt Lett 36(22):4380–4382
8. Wang XD, Wolfbeis OS (2016) Fiber-optic chemical sensors and biosensors (2013-2015). Anal Chem 88(1):203–227
9. Wang XD, Wolfbeis OS (2019) Fiber-Optic Chemical Sensors and Biosensors (2015-2019). Anal Chem, on the web. DOI: https://doi.org/10.1021/acs.analchem.9b04708
10. Guo T, Liu F, Liang X, Qiu X, Huang Y, Xie C, Xu P, Mao W, Guan BO, Albert J (2016) Highly sensitive detection of urinary protein variations using tilted fiber grating sensors with plasmonic nanocoatings. Biosens Bioelectron 78:221–228
11. Hromadka J, Tokay B, James S, Tatam RP, Korposh S (2015) Optical fibre long period grating gas sensor modified with metal organic framework thin films. Sensor Actuat B-Chem 221:891–899
12. Jorgenson RC, Yee SS (1993) A fiber-optic chemical sensor based on surface plasmon resonance. Sensors Actuators B Chem 12(3):213–220
13. Katarzyna G, Tadeusz M, Maciej N, Kinga Z, Pawel M, Waclaw U (2017) A surface plasmon resonance sensor based on a single mode D-shape polymer optical fiber. J Opt 19(2):025001
14. Lee B, Park J-H, Byun J-Y, Kim JH, Kim M-G (2018) An optical fiber-based LSPR aptasensor for simple and rapid in-situ detection of ochratoxin a. Biosens Bioelectron 102:504–509
15. Menon PS, Said FA, Mei GS, Berhanuddin DD, Umar AA, Shaari S, Majlis BY (2018) Urea and creatinine detection on nano-laminated gold thin film using Kretschmann-based surface plasmon resonance biosensor. PLoS One 13(7):e0201228–e0201228
16. Mishra S K, Gupta B D, Surface plasmon resonance (SPR) based fiber optic urea sensor using silver, ITO and enzyme entrapped gel layers, in: Frontiers in Optics 2014, Optical Society of America, Tucson, Arizona, 2014, pp. FTu5B.3
17. Yin MJ, Huang B, Gao S, Zhang AP, Ye X (2016) Optical fiber LPG biosensor integrated microfluidic chip for ultrasensitive glucose detection. Biomed Opt Express 7(5):2067–2077
18. Tan Y, Sun L-P, Jin L, Li J, Guan B-O (2013) Microfiber Mach-Zehnder interferometer based on long period grating for sensing applications. Opt Express 21(1):154–164
19. Li K, Liu G, Wu Y, Hao P, Zhou W, Zhang Z (2014) Gold nanoparticle amplified optical microfiber evanescent wave absorption biosensor for cancer biomarker detection in serum. Talanta 120(Supplement C):419–424
20. Tripathi SM, Kumar A, Varshney RK, Kumar YBP, Marin E, Meunier JP (2009) Strain and temperature sensing characteristics of single-mode-multimode-single-mode structures. J Lightwave Technol 27(13):2348–2356
21. Liu ZB, Tan Z, Yin B, Bai Y, Jian S (2014) Refractive index sensing characterization of a singlemode-claddingless-singlemode fiber structure based fiber ring cavity laser. Opt Express 22(5):5037–5042
22. Tyagi D, Mishra SK, Zou B, Lin C, Hao T, Zhang G, Lu A, Chiang KS, Yang Z (2018) Nano-functionalized long-period fiber grating probe for disease-specific protein detection. J Mater Chem B 6(3):386–392
23. Tam JM, Song L, Walt DR (2009) DNA detection on ultrahigh-density optical fiber-based nanoarrays. Biosens Bioelectron 24(8):2488–2493
24. Jiang B, Zhou K, Wang C, Sun Q, Yin G, Tai Z, Wilson K, Zhao J, Zhang L (2018) Label-free glucose biosensor based on enzymatic graphene oxide-functionalized tilted fiber grating. Sensors and Actuators B: Chemical 254(Supplement C):1033–1039
25. Baliyan A, Bhatia P, Gupta BD, Sharma EK, Kumari A, Gupta R (2013) Surface plasmon resonance based fiber optic sensor for the detection of triacylglycerides using gel entrapment technique. Sensors Actuators B Chem 188:917–922
26. Liang K, Ricco R, Doherty CM, Styles MJ, Bell S, Kirby N, Mudie S, Haylock D, Hill AJ, Doonan CJ, Falcaro P (2015) Biomimetic mineralization of metal-organic frameworks as protective coatings for biomacromolecules. Nat Commun 6:7240
27. Lyu F, Zhang Y, Zare RN, Ge J, Liu Z (2014) One-pot synthesis of protein-embedded metal–organic frameworks with enhanced biological activities. Nano Lett 14(10):5761–5765
28. Shieh F-K, Wang S-C, Yen C-I, Wu C-C, Dutta S, Chou L-Y, Morabito JV, Hu P, Hsu M-H, Wu KCW, Tsung C-K (2015) Imparting functionality to biocatalysts via embedding enzymes into Nanoporous materials by a de novo approach: size-selective sheltering of catalase in metal–organic framework microcrystals. J Am Chem Soc 137(13):4276–4279
29. Nazari M, Forouzandeh MA, Divarathne CM, Sidiroglou F, Martinez MR, Konstas K, Muir BW, Hill AJ, Duke MC, Hill MR, Collins SF (2016) UiO-66 MOF end-face-coated optical fiber in aqueous contaminant detection. Opt Lett 41(8):1696–1699
30. Hou C, Wang Y, Ding Q, Jiang L, Li M, Zhu W, Pan D, Zhu H, Liu M (2015) Facile synthesis of enzyme-embedded magnetic metal-organic frameworks as a reusable mimic multi-enzyme system: mimetic peroxidase properties and colorimetric sensor. Nanoscale 7(44):18770–18779
31. Wu X, Yang C, Ge J, Liu Z (2015) Polydopamine tethered enzyme/metal-organic framework composites with high stability and reusability. Nanoscale 7(45):18883–18886
32. Doonan C, Riccò R, Liang K, Bradshaw D, Falcaro P (2017) Metal–organic frameworks at the biointerface: synthetic strategies and applications. Acc Chem Res 50(6):1423–1432

33. Alqasaimeh M, Heng LY, Ahmad M, Raj AS, Ling TL (2014) A large response range reflectometric urea biosensor made from silica-gel nanoparticles. Sensors (Basel) 14(7):13186–13209
34. Swati M, Hase NK, Srivastava R (2010) Nanoengineered optical urea biosensor for estimating hemodialysis parameters in spent dialysate. Anal Chim Acta 676(1):68–74
35. Bhatia P, Gupta BD (2012) Fabrication and characterization of a surface plasmon resonance based fiber optic urea sensor for biomedical applications. Sensors Actuators B Chem 161(1): 434–438
36. de Marcos S, Hortigüela R, Gatbán J, Castillo J R, Wolfbeis O S J M A (1999) Characterization of a urea optical sensor based on polypyrrole. 130(4):267–272
37. Mehta J, Bhardwaj N, Bhardwaj SK, Kim K-H, Deep A (2016) Recent advances in enzyme immobilization techniques: metal-organic frameworks as novel substrates. Coordination Chemistry Reviews 322(Supplement C):30–40

Publisher's note Springer Nature remains neutral with regard to jurisdictional claims in published maps and institutional affiliations.